Deformation Induced Semiconductor-Metal Transition in Single Wall Carbon Nanotubes Probed by Electric Force Microscopy

A. P. M. Barboza, A. P. Gomes, B. S. Archanjo, P. T. Araujo, A. Jorio, A. S. Ferlauto,
M. S. C. Mazzoni, H. Chacham, and B. R. A. Neves[*]

Departamento de Física, ICEX, Universidade Federal de Minas Gerais, CP 702, 30123-970, Belo Horizonte, MG, Brazil
(Received 8 February 2008; published 27 June 2008)

We report the direct experimental observation of the semiconductor-metal transition in single-wall carbon nanotubes (SWNTs) induced by compression with the tip of an atomic force microscope. This transition is probed via electric force microscopy by monitoring SWNT charge storage. Experimental data show that such charge storage is different for metallic and semiconducting SWNTs, with the latter presenting a strong dependence on the tip-SWNT force during injection. *Ab initio* calculations corroborate experimental observations and their interpretation.

The intriguing properties of carbon nanotubes have been scrutinized by a host of researchers, which have harvested enormous amounts of important information [1–17]. In particular, the ability of SWNTs to change their electrical conductance due to mechanical deformation received attention from both theoretical and experimental works, evidencing the potential use of SWNTs in device fabrication [1–4,8–14]. The semiconductor-metal transition in semiconducting SWNTs due to radial compression is a good example. Although predicted several years ago [2–4] there is a single, indirect, piece of experimental evidence of this effect (in accidentally deformed SWNTs) in the literature [5]. In this Letter, we report the direct experimental observation of this effect via electric force microscopy (EFM).

Isolated SWNTs were grown by CVD on a 100 nm-thick SiO_x layer on top of a *p*-doped Si substrate using Fe nanoparticles as catalyzers. After growth, each lithographically marked sample is characterized via backscattering micro Raman spectroscopy enabling the semiconductor-metallic characterization and a probable (n, m) indexing of the SWNTs [6,7,18]. Then, each Raman-labeled SWNT is imaged by AFM to check its morphology and, finally, the charging experiment takes place. Scanning probe microscopy measurements were carried out under dry nitrogen atmospheres (in most cases), or in air (in some cases) with the help of homemade environmental control chambers. AuCr-covered silicon cantilevers with nominal spring constant $k \sim 0.3$ to 0.6 N/m, nominal radius of curvature $R \sim$ 30 nm and resonant frequency $\omega_0 \sim 20$ to 40 kHz were employed throughout this work for AFM (contact and intermittent contact modes) and EFM characterization. More accurate estimations of k and R were carried out by the use of the Sader's method [19] and by imaging reference samples, respectively.

Figure 1(a) describes schematically the charging process: the SWNT is charged through contact with a properly biased (V_{INJ}) AFM tip [15–17]. Both tip bias V_{INJ} and tip-

SWNT force F during the charging process can be easily controlled, while tip-SWNT contact time t_{INJ} is kept fixed ($t_{INJ} = 1$ s) [15–17]. Differently from previous studies on SWNT charging, no bias is applied between tip and sample during the second pass (EFM) imaging [15–17]. Therefore, the extra SWNT charges induce image charges of opposite sign in the EFM tip during the second pass, leading to an attractive tip-sample interaction which shifts the cantilever oscillation frequency to lower values [20]. Figures 1(b) and 1(c) show typical AFM and EFM images of SWNTs investigated in this work. Like the (14,6) semiconducting nanotube shown in Fig. 1(b), all SWNTs are from several hundreds nanometers to a few microns long placed atop a clean SiO_x surface. Its EFM image in Fig. 1(c) shows the negative frequency shift of the cantilever (down to dark blue colors) relative to the uncharged SiO_x surface (in orange), demonstrating the presence of unbalanced charges in this SWNT [15–17,20]. Figure 1(c) also shows that the charge, in spite of being injected in the SWNT on a specific location [see Fig. 1(a)], is uniformly distributed along the SWNT length [15–17].

The amount of unbalanced charges in a given SWNT can be estimated from EFM images through a simple model considering the electric field of a long one-dimensional wire carrying a charge density λ per unit length. The general theory of EFM shows that the frequency shift $\Delta\omega$ measured in EFM images is directly related to the gradient of the electrostatic tip-sample force F' due to the electric field E by $\Delta\omega = \omega_0 (2k)^{-1} F'$, where ω_0 and k are the cantilever resonant frequency and spring constant, respectively [20]. Therefore, the charge density per unit length λ in a SWNT is related to the frequency shift $\Delta\omega$ measured in EFM images by $\lambda = (4\pi\epsilon k z^2 \omega_0^{-1} L_{ef}^{-1} \Delta\omega)^{1/2}$, where z is the tip-SWNT distance during EFM imaging, ϵ is the electrical permittivity of the air, and L_{ef} is the effective length of tip-SWNT interaction. As a first approximation, L_{ef} can be taken either as the tip diameter or as the tip-SWNT distance, whichever is larger. For the conditions of
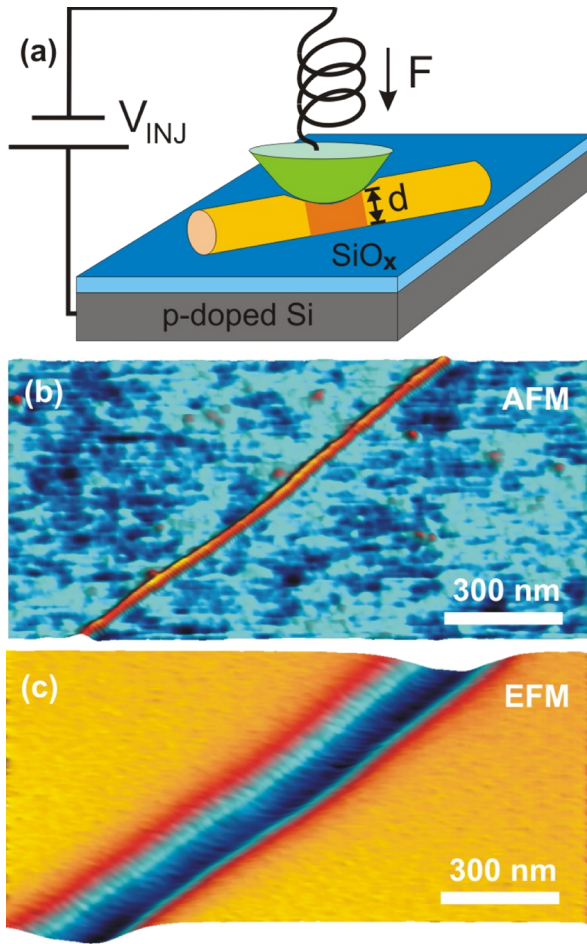
FIG. 1 (color online). (a) Schematic drawing representing the experiment: a SWNT (in orange) on top a silicon oxide layer (in blue) is charged through the contact with an AFM tip (in green) biased at V_{INJ} while it is pressed with a controlled force per unit length F. (b) 3D AFM image of a (14,6) semiconducting SWNT atop the SiO_x layer. (c) 3D EFM image of the same nanotube after it has been charged ($V_{INJ} = 6$ V, lift height = 50 nm) evidencing the negative frequency shift of the cantilever.

the present work, the tip-SWNT distance during EFM measurements is always larger than the tip diameter.

The compressive force per unit length exerted by the AFM tip onto a SWNT was estimated through a simple procedure: initially, the total compressive tip force F is calculated via conventional force-distance plots [19]. Then, an AFM image of the investigated SWNT is acquired and since SWNT radius is more than an order of magnitude smaller than tip radius, the apparent nanotube width is actually, due to the strong convolution, a depiction of the tip apex [20]. Therefore, the tip-SWNT contact length is estimated simply by measuring the nanotube apparent width (the Full-Width-at-Half-Maximum of the nanotube AFM profile).

In order to search for the semiconductor-metal transition in SWNTs, two experiments were devised: initially, a pair of Raman-labeled metallic and semiconducting SWNTs with similar diameters is chosen and a survey of the

injected charge on each SWNT as a function of tip bias V_{INJ} is carried out. In this experiment, the tip-SWNT compressive force F is kept at a minimum value, which is enough to assure good electric contact between them, but does not cause any significant deformation of the nanotube [11]. In the present experiments, F per unit SWNT length is kept between 0.2 N/m and 0.4 N/m. Figure 2(a) shows the detected linear charge density λ as a function of tip bias V_{INJ} for a (14,6) semiconducting SWNT (red triangles) and a (10,7) metallic SWNT (black squares). Similar plots for several metallic and semiconducting SWNTs with different chiralities were produced during this work and all of them present the same features: metallic SWNTs always present a symmetric charge-bias plot and a minimum bias of $\sim \pm 2$ V is necessary for unbalanced charges to be detected at the nanotube. Such observation is an intrinsic effect [21,22] and is not related to any poor electrical contact between tip and nanotube as shown at the $I(V)$
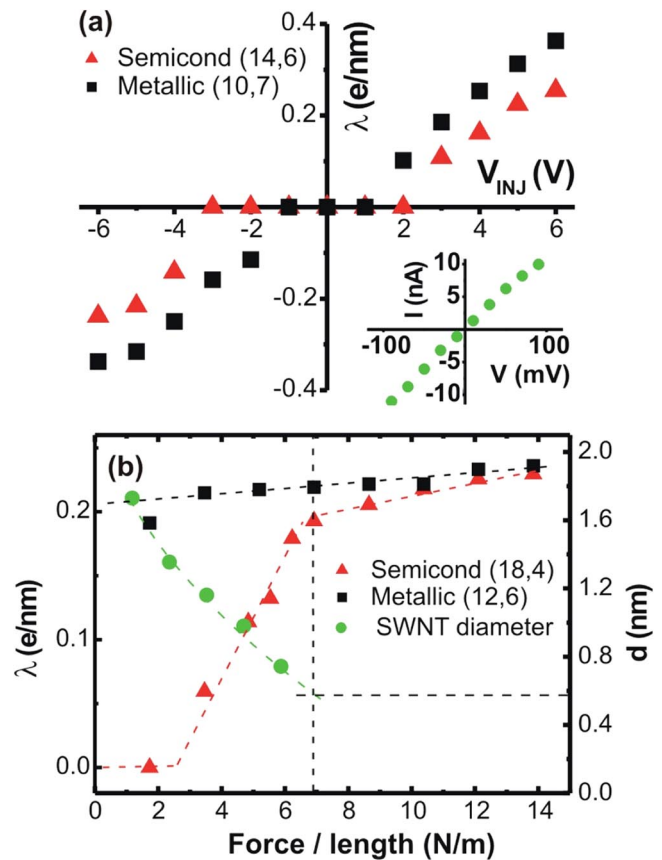
FIG. 2 (color online). (a) Plot of the charge density λ (in electrons/nm) as a function of injection bias V_{INJ} for a (10,7) metallic nanotube (black squares) and a (14, 6) semiconducting nanotube (red triangles). The inset shows an I(V) curve acquired with the tip in contact with a thin metallic (Mo) film. (b) Plot of the charge density λ as function of the applied compressive force per unit length for (12,6) metallic nanotube (black squares) and (18,4) semiconducting nanotube (red triangles). The evolution of the apparent height (diameter) of the (18,4) semiconducting SWNT with applied force is also plotted in this graph (green circles). The dashed lines are guides for the eye.

curve in the inset of Fig. 2(a). This curve, acquired with the tip in contact with a thin metallic film at the same tip-sample force of the plots in Fig. 2(a), evidences the Ohmic nature of the tip-sample contact even at low bias (the observed resistance of ~10 MΩ is simply the series resistance of the current measurement circuit). Nevertheless, Fig. 2(a) shows an important difference when comparing metallic and semiconducting SWNTs: charging semiconducting SWNTs is nonsymmetrical with respect to bias (the bias threshold is always larger for negative tip bias V_{INJ}) and for a given bias, the detected linear density of unbalanced charges is also smaller for semiconducting nanotubes [18]. It is important to note in Fig. 2(a) the strikingly different behavior of these two nanotubes at bias $V_{INJ} = -3$ V: while the metallic SWNTs shows a substantial charge density, no charge at all is injected/detected in the semiconducting nanotube. Therefore, such bias condition presents an ideal prospect for the second devised experiment: keeping both bias V_{INJ} and tip-SWNT contact time t_{INJ} constant, the injected charge density on each nanotube is monitored as a function of the compressive tip-SWNT force during injection. Again, this experiment was repeated several times for different metallic and semiconducting SWNTs with similar results which are typically represented by the plots in Fig. 2(b). This figure, acquired for a (12,6) metallic and a (18,4) semiconducting nanotubes, shows the measured charge density λ as a function of the compressive force per unit length applied onto each nanotube by the tip. The metallic SWNT (black squares) presents only a weak dependence of the tip force on the charging process, while for a semiconducting SWNT, such charging is strongly force dependent: for small forces per unit length (~2 N/m), no charge is detected at the SWNT [as expected from Fig. 2(a)]. When the compressive force is increased between 3 N/m and 7 N/m, a remarkable effect is observed: a steady increase of the stored charge per unit length in the semiconducting SWNT (red triangles). When the tip compressive force per unit length is increased further, above 8 N/m, a saturation is observed, achieving similar charge densities of the metallic SWNT at such forces. Therefore, the data in Fig. 2(b) indicates a transition of the semiconducting SWNT to a metallic behavior as it is compressed. In order to gain further insights into this effect, the semiconducting SWNT was imaged in contact-mode AFM and its apparent diameter d (height) was measured as a function of the applied compressive tip force. The diameter evolution with force is also plot in Fig. 2(b) (green circles), showing its steady decrease as the nanotube is further compressed (up to 6 N/m) [23]. The experimental results shown in Fig. 2(b) indicate that the energy barrier for charge injection from the AFM tip into the (18,4) nanotube becomes similar to that of the (12,6) metallic nanotube for compression forces larger than 7 N/m. We claim that, at this point, the bandgap of the (18,4) nanotube vanishes and the tube becomes metallic.

Is this assumption supported by theory? Indeed, the bandgap closure of semiconducting nanotubes upon radial deformation has long been theoretically predicted [2−4]. In order to gain further insight on this phenomenon, we performed *ab initio* calculations for the (20,0) and the (18,4) nanotubes, which have similar diameters. These calculations are performed with the pseudopotential density functional theory [24−26] within the generalized gradient approximation [27] as implemented in the SIESTA [28,29] code. In our calculations, the nanotube cross section was progressively flattened following the model described in Ref. [2], leading to structures as the one shown in Fig. 3(a), which are characterized by the flattening distance (height) d. The behavior of the energy gap as a function of d is depicted in Fig. 3(b) for the (20,0) nanotube, and it indicates a semiconductor-metal transition at $d = 0.55$ nm. We also performed calculations of the compressive force on the (20,0) nanotube. This was carried out in two different ways: first, from the total energy E, which behaves as d^{-1}, as shown in a previous work [2]. We fit E to a curve $E = E_0 + a/d$ and take the derivative with respect to d. This is shown in the inset of Fig. 3(b) as a straight black line. This procedure leads to a calculated semiconductor-metal transition at $F = 4.4$ N/m. The total force can also be directly obtained in the first-principles calculations by summing up the components of the remanent forces in the flattening direction over the atoms of the
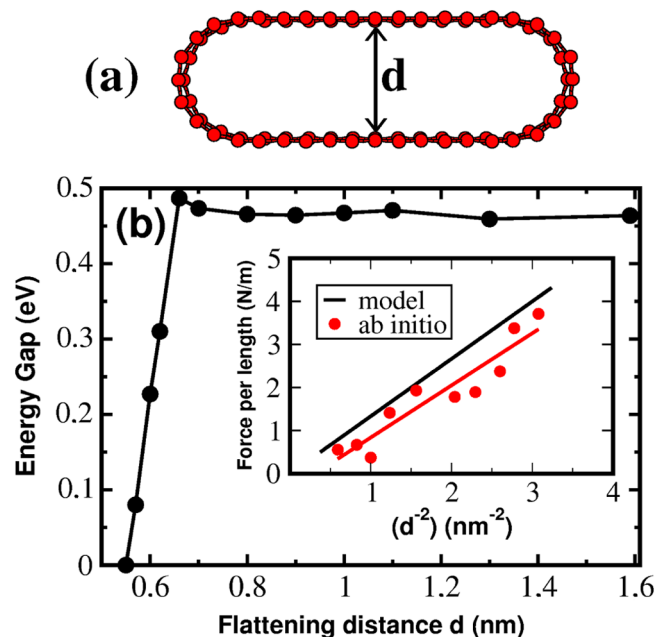
FIG. 3 (color online). (a) Calculated optimized geometry of a flattened (20,0) SWNT, characterized by a compressed diameter $d = 0.66$ nm. (b) Calculated bandgap of the (20,0) SWNT as a function of its compressed diameter d showing a semiconductor-metal transition at $d = 0.55$ nm. The inset shows the compressive force per unit length, calculated both from the fitting of the total energy to $E = E_0 + a/d$ (black line) and directly from the constraint forces (red circles).

upper (or lower) constraint region. This is also shown in the inset of Fig. 3(b). This second procedure leads to a metallization of the (20,0) nanotube at $F = 4.0$ N/m, consistent with the first one, and also consistent with the "onset" of the transition in Fig. 2(b). The 824-atom unit cell of the (18,4) nanotube prevents a high-level *ab initio* calculation for this nanotube. However, semiquantitative trends may be obtained with a smaller basis set (minimal basis). Such calculations for the (18,4) nanotube indicate that a semiconductor-metal transition will take place, however at a larger compression ($d \sim 0.4$ nm). Considering the d^{-2} dependence of the applied force, this would imply in a critical force ($F/l \sim 8$ N/m) that is almost twice as the calculated one for the (20,0) nanotube, and that would be more consistent with the "end" of the transition in Fig. 2(b). Altogether, the analysis for the (20,0) and the trends for the (18,4) nanotube reinforces the assumption of a semiconductor-metal transition induced by compression as responsible for the charging injection results observed in the experiment.

In conclusion, this Letter reports on a direct experimental observation of a long-predicted semiconductor-metal transition in SWNTs. It is important to note that such transition is completely reversible: once the compressive force ceases, the SWNT recovers its original semiconducting character. Therefore, for a given semiconducting nanotube, it is possible to create reversible semiconductor-metal junctions at will along its length. Such result may open up several design possibilities for electrical devices, dynamically changing charge transport properties along the SWNT through the application of a "force gate" [8,11,12,22]. Finally, as a by-product of the present work, the developed method (monitor unbalanced charges in SWNT as functions of bias and compressive force) turns out to be a reliable method for easy determination of the metallic/semiconducting character of any given SWNT. In other words, there is no need of tedious lithography processes to check one, or a few, SWNTs of a given batch through I(V) characterization, nor it has the limitation of discriminating only SWNTs which, by chance, happen to be in resonance, and with the right orientation, with a laser beam; the present methodology can be applied to any SWNT, assessing its metallic/semiconducting character on a process-free as-grown sample.

*bernardo@fisica.ufmg.br

[1] A. Jorio, M. S. Dresselhaus, and G. Dresselhaus, *Carbon Nanotubes: Advanced Topics in Synthesis, Properties and Applications*, Topics in Applied Physics Vol. 111 (Springer, Berlin, 2007).
[2] M. S. C. Mazzoni and H. Chacham, Appl. Phys. Lett. **76,** 1561 (2000).
[3] C.-J. Park *et al.*, Phys. Rev. B **60,** 10656 (1999).
[4] B. Shan *et al.*, Appl. Phys. Lett. **87,** 173109 (2005).
[5] L. Vitali *et al.*, Phys. Rev. Lett. **96,** 086804 (2006).
[6] A. Jorio *et al.*, Phys. Rev. Lett. **86,** 1118 (2001); P. T. Araujo *et al.*, *ibid.* **98,** 067401 (2007).
[7] Note that Raman data unambiguously separate metallic from semiconducting nanotubes, which is the important issue in the present work, but the exact (n, m) assignment may be compromised by nanotube-substrate interaction [1]. Nevertheless, the (n, m) nominal assignment is kept in the text to single out each nanotube.
[8] T. W. Tombler *et al.*, Nature (London) **405,** 769 (2000).
[9] E. D. Minot *et al.*, Phys. Rev. Lett. **90,** 156401 (2003).
[10] J. Cao *et al.*, Phys. Rev. Lett. **90,** 157601 (2003).
[11] C. Gómez-Navarro *et al.*, Adv. Mater. **16,** 549 (2004).
[12] C. Gómez-Navarro *et al.*, Phys. Rev. Lett. **96,** 076803 (2006).
[13] T. Cohen-Karni *et al.*, Nature Nanotechnology **1,** 36 (2006).
[14] A. R. Hall *et al.*, Nature Nanotechnology **2,** 413 (2007).
[15] M. Paillet *et al.*, Phys. Rev. Lett. **94,** 186801 (2005).
[16] M. Zdrojek *et al.*, Appl. Phys. Lett. **86,** 213114 (2005).
[17] M. Zdrojek *et al.*, J. Appl. Phys. **100,** 114326 (2006).
[18] See EPAPS Document No. E-PRLTAO-101-055852 for Raman spectra of all four SWNTs used to produce the data in Fig. 2 and also a phenomenological model explaining some features of Fig. 2(a) (charge-bias threshold, charging asymmetry for semiconducting SWNT and influence of the Au/SWNT contact nature). For more information on EPAPS, see http://www.aip.org/pubservs/epaps.html.
[19] J. E. Sader *et al.*, Rev. Sci. Instrum. **70,** 3967 (1999).
[20] D. A. Bonnell, *Scanning Probe Microscopy and Spectroscopy* (Wiley-VCH, New York, 2001).
[21] C. Baldacchini *et al.*, Appl. Phys. Lett. **91,** 122103 (2007).
[22] Y. Yaish *et al.*, Phys. Rev. Lett. **92,** 046401 (2004).
[23] It was not possible to image this nanotube at larger compressive forces as it was dragged by the tip at such high forces precluding any reliable imaging.
[24] W. Kohn and L. J. Sham, Phys. Rev. **140,** A1133 (1965).
[25] N. Troullier *et al.*, Phys. Rev. B **43,** 1993 (1991).
[26] L. Kleinman *et al.*, Phys. Rev. Lett. **48,** 1425 (1982).
[27] J. P. Perdew *et al.*, Phys. Rev. Lett. **77,** 3865 (1996).
[28] J. M. Soler *et al.*, J. Phys. Condens. Matter **14,** 2745 (2002).
[29] For the (20,0) nanotube, the wave functions are expanded in a double-zeta basis set composed of pseudoatomic orbitals of finite range augmented by polarization functions. The confinement radii are defined by a common energy shift in the atomic orbitals of 0.01 Ry. The grid in the real space is defined by a mesh cutoff of 200 Ry. All geometries are relaxed until the maximum force component is less than 0.02 eV/Å. For the (18,4) nanotube, a minimal basis set is employed.